Electronic Supplementary Information

Nanoboxes with Porous MnO Core and Amorphous TiO_2 Shell as Mediator for Lithium-Sulfur Battery

Jinhua Yang,[1] Xianfeng Yang,[1] Jian Liang Cheong,[1] Karim Zaghib,[2] Michel L. Trudeau,[3] and Jackie Y. Ying[1]*

[1]*NanoBio Lab, Agency for Science, Technology and Research, 31 Biopolis Way, The Nanos, Singapore 138669.*

[2]*Department of Mining and Materials Engineering, McGill University, 845 Sherbrooke Street West, Montréal, QC, Canada H3A 0G4.*

[3]*Center of Excellence in Transportation, Electrification and Energy Storage, Hydro-Québec, 1806 Bd. Lionel-Boulet, Varennes, QC, Canada J3X 1S1.*

**E-mail:* jyying@nbl.a-star.edu.sg.

Table S1. ICP-OES result of MnO@TiO_2 and MnO@TiO_2/RGO-acid

Sample	Ti	Mn	Ti:Mn Molar Ratio
MnO-TiO_2	14.43	50.51	1:3.5
MnO-TiO_2/RGO-acid	19.71	25.35	1:1.3

Table S2. Comparison of recent reports on sulfur host cathodes with MnO@TiO_2/RGO-acid for Li-S battery.

Host materials	Capacity (mAh/g) (current rate)	Cycling stability (%) (cycles, current rate)	Decay rate per cycle (%)	Reference
ZnS/NC	1232 (0.2 C)	66.7% (200, 0.2 C)	0.19	1
CoP@HCP	1058.2 (0.1 C)	84.8% (200, 0.2 C)	0.08	2
NiO-$NiCo_2O_4$@HC	1063.2 (0.2 C)	70.5% (500, 0.5 C)	0.06	3
NiS@C-HS	1196 (0.1 C)	72.0% (200, 0.2 C)	0.14	4
MnO@TiO_2/RGO-acid	1451 (0.1 C)	74.3% (500, 0.5 C)	0.05	This Work

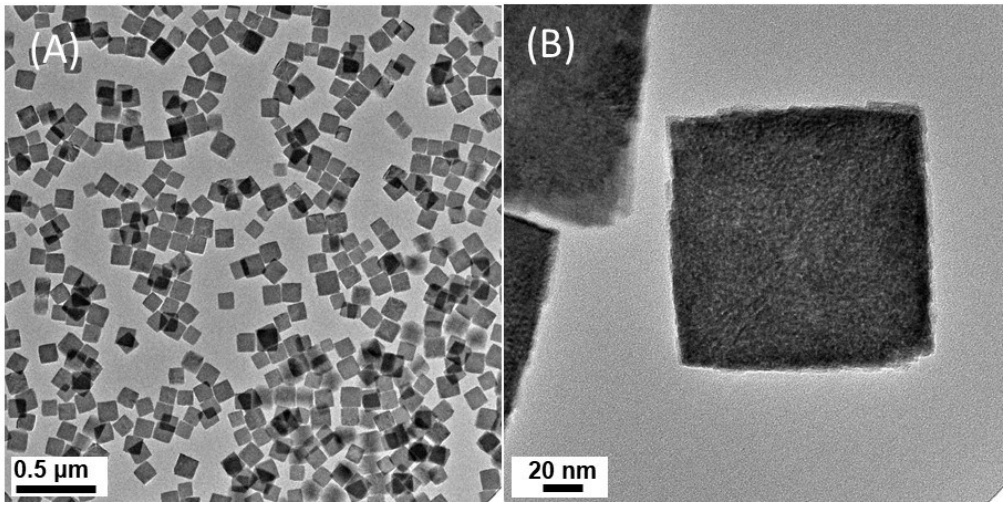

Fig. S1. (A) Low- and (B) high-magnification TEM images of $MnCO_3$ nanocubes.

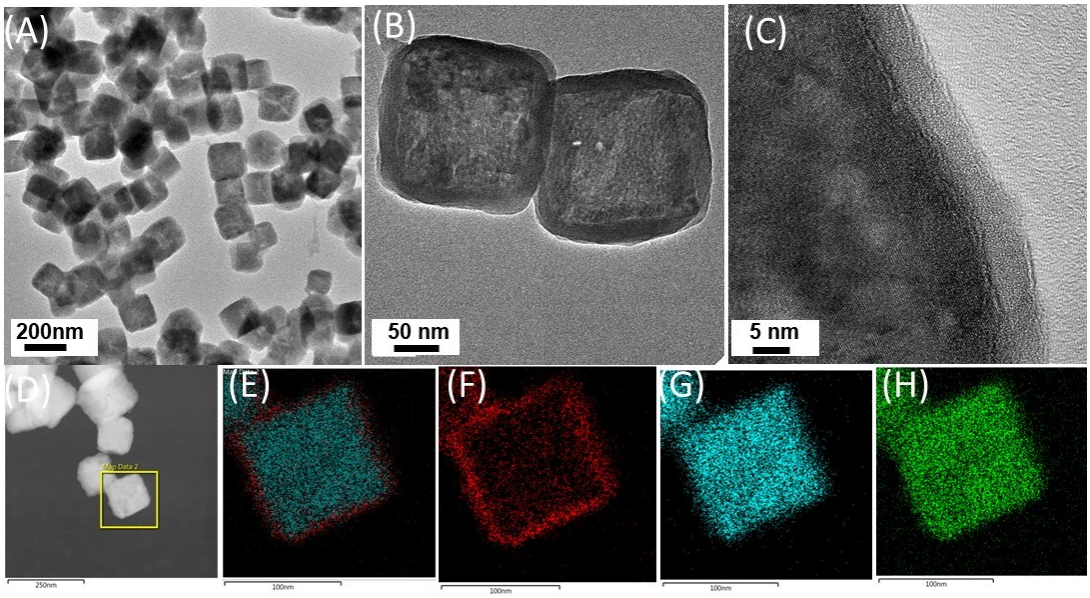

Fig. S2. (A) TEM, (B, C) HRTEM and (D) HAADF-STEM images of $MnCO_3$@TiO_2 nanocubes. (E) Ti and Mn, (F) Ti, (G) Mn and (H) O EDX maps of the boxed $MnCO_3$@TiO_2 nanocube in (D).

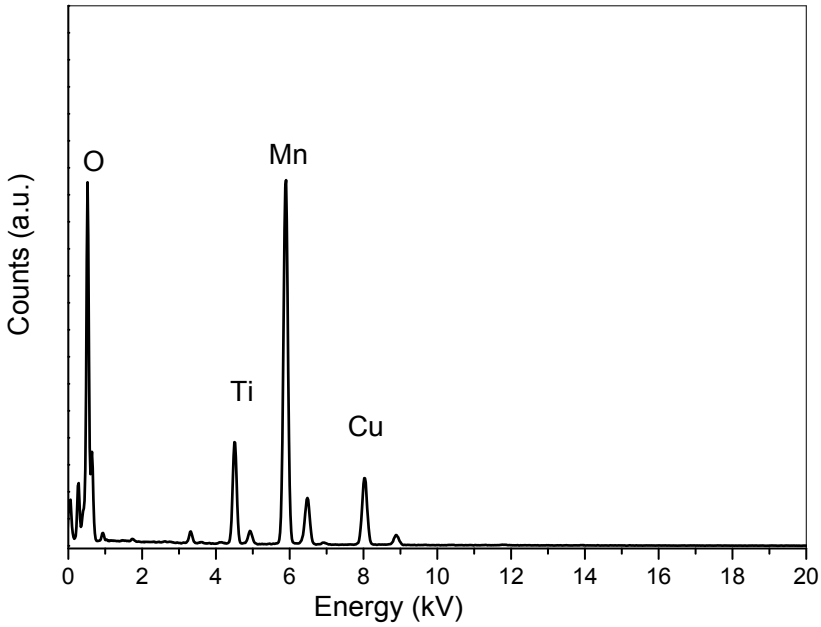

Fig. S3. EDX profile of MnO@TiO_2. The Ti:Mn molar ratio was determined to be ~ 1:4.

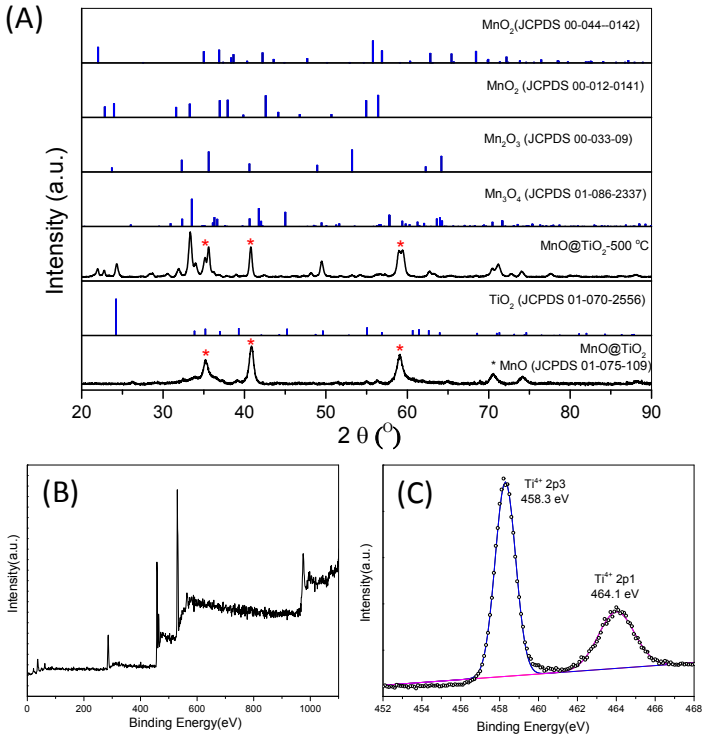

Fig. S4. (A) XRD pattern of MnO@TiO_2 annealed at 350ºC and 500ºC. After annealing at 500ºC, MnO_2, Mn_2O_3 and Mn_3O_4 phases were found besides MnO phase, and crystalline TiO_2 phase was also detected. (B, C) XPS spectra of MnO@TiO_2 (annealed at 350ºC).

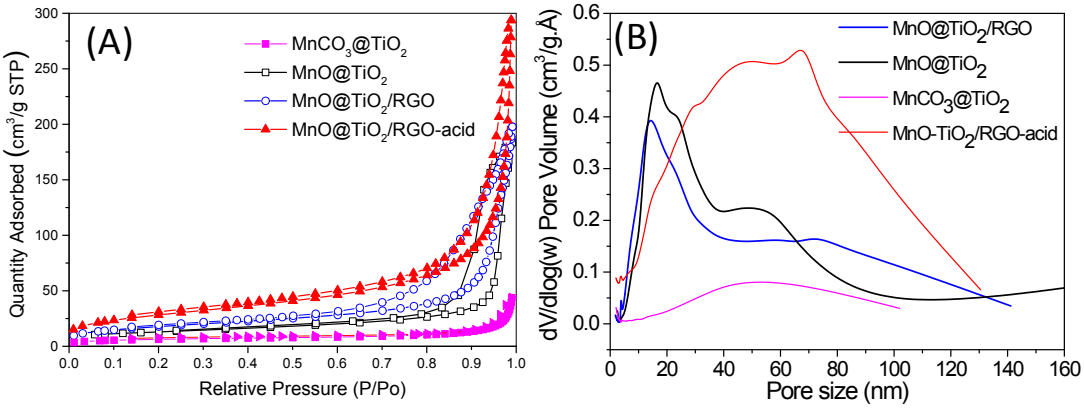

Fig. S5. (A) N_2 adsorption/desorption isotherms and (B) pore size distribution curves of $MnCO_3$@TiO_2, MnO@TiO_2, MnO@TiO_2/RGO and MnO@TiO_2/RGO-acid.

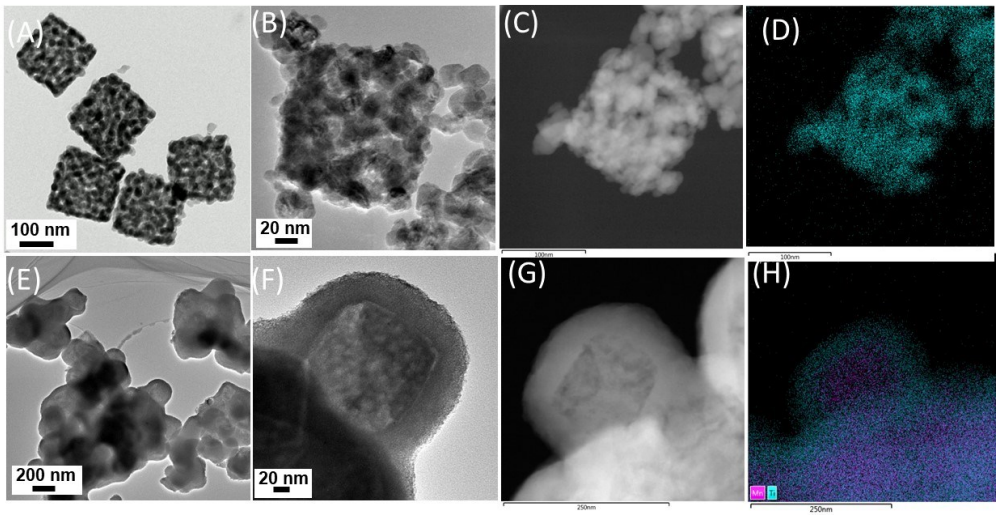

Fig. S6. (A, E) TEM and (B, F) HRTEM images, (C, G) HAADF-STEM images and (D, H) EDX elemental maps of (A–D) MnO and (E–H) MnO@TiO_2 synthesized with 1.5 mL of Ti(IV) butoxide.

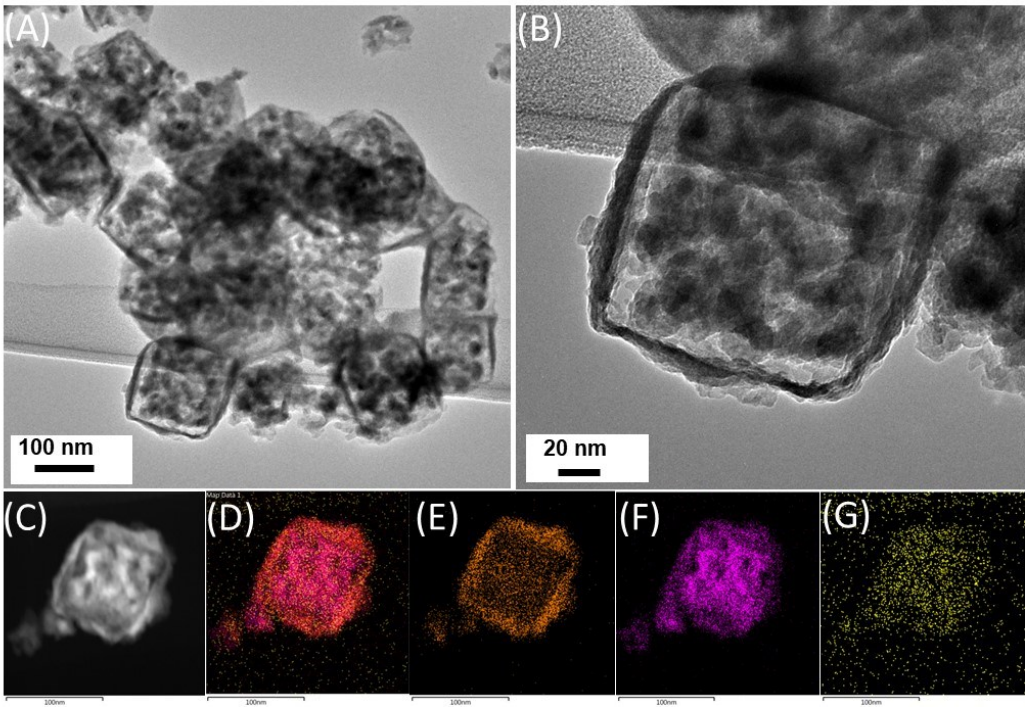

Fig. S7. (A) TEM, (B) HRTEM and (C) HAADF-STEM images of $MnO@TiO_2$-S nanocomposites. (D) Ti and Mn, (E) Ti, (F) Mn and (G) O EDX maps of the $MnO@TiO_2$-S nanocomposite in (C).

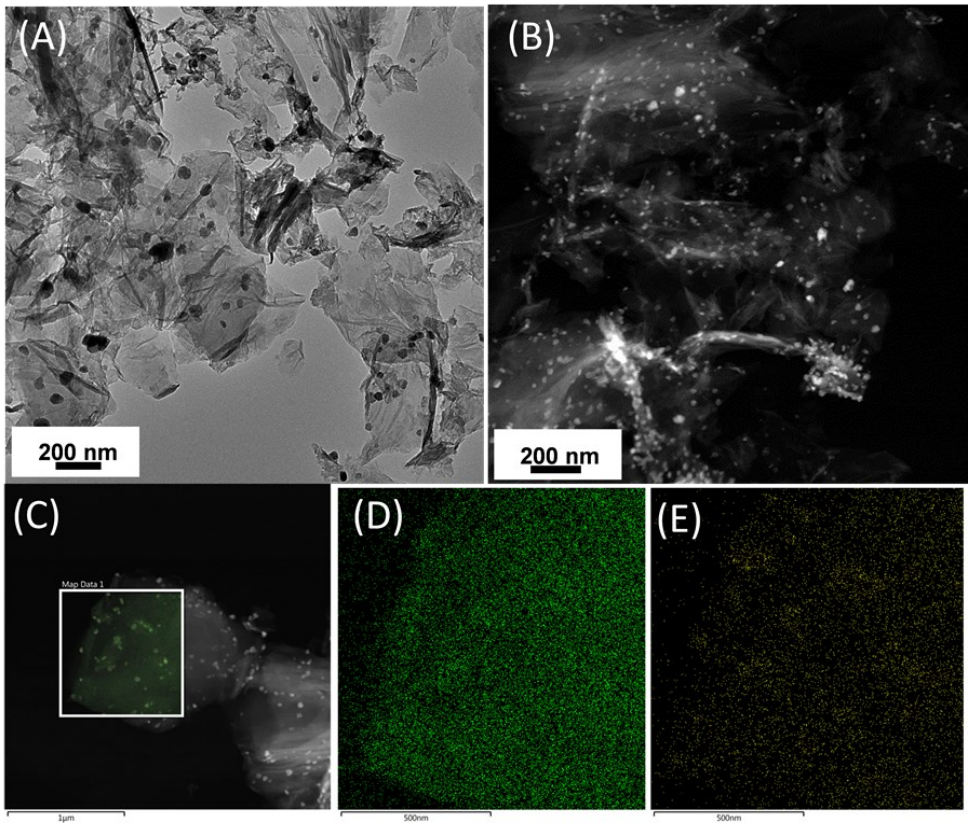

Fig. S8. (A) TEM and (B, C) HAADF-STEM images of RGO-S nanocomposites. (D) C and (E) S maps of the boxed RGO-S nanocomposites in (C).

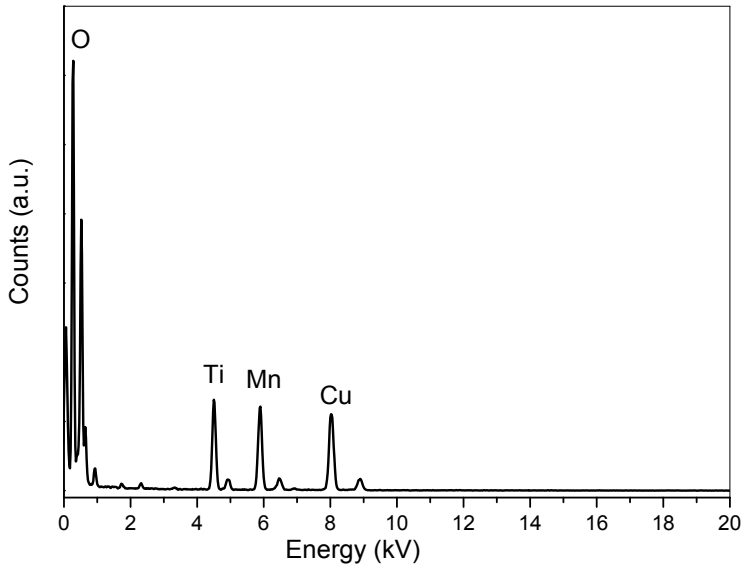

Fig. S9. EDX profile of $MnO@TiO_2$/RGO-acid. The Ti:Mn molar ratio was determined to be ~ 1:1.

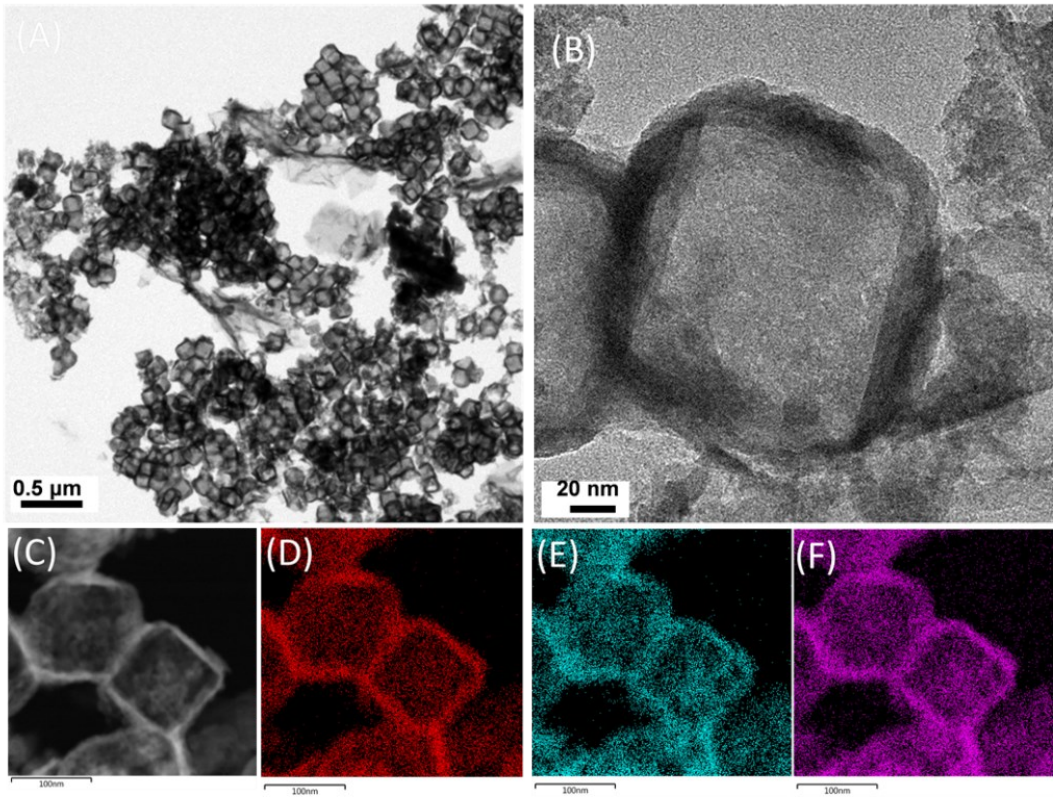

Fig. S10. (A) Low- and (B) high-magnification TEM, and (C) HAADF-STEM images of $MnO@TiO_2$/RGO-acid nanocomposites. (D) Ti, (E) Mn and (F) O EDX maps of the $MnO@TiO_2$/RGO-acid nanocomposites in (C).

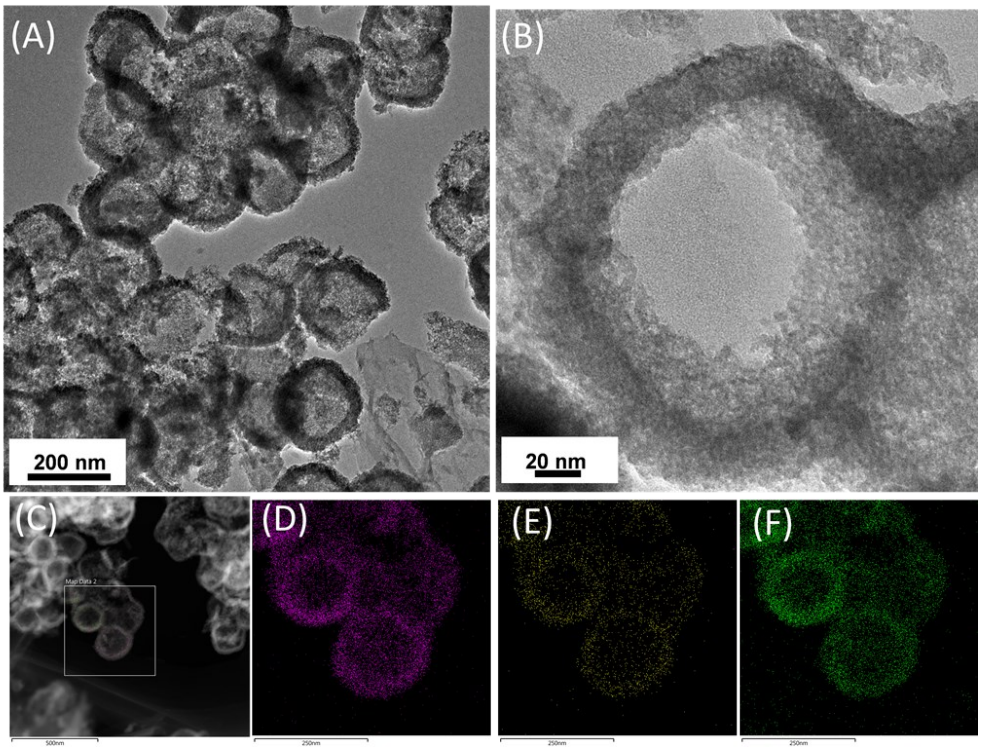

Fig. S11. (A) Low- and (B) high-magnification TEM, and (C) HAADF-STEM images of MnO@TiO_2/RGO-acid-hollow nanocomposites obtained with 24 h of reaction. (D) Ti, (E) Mn and (F) O maps of the boxed MnO@TiO_2/RGO-acid-hollow nanocomposites in (C).

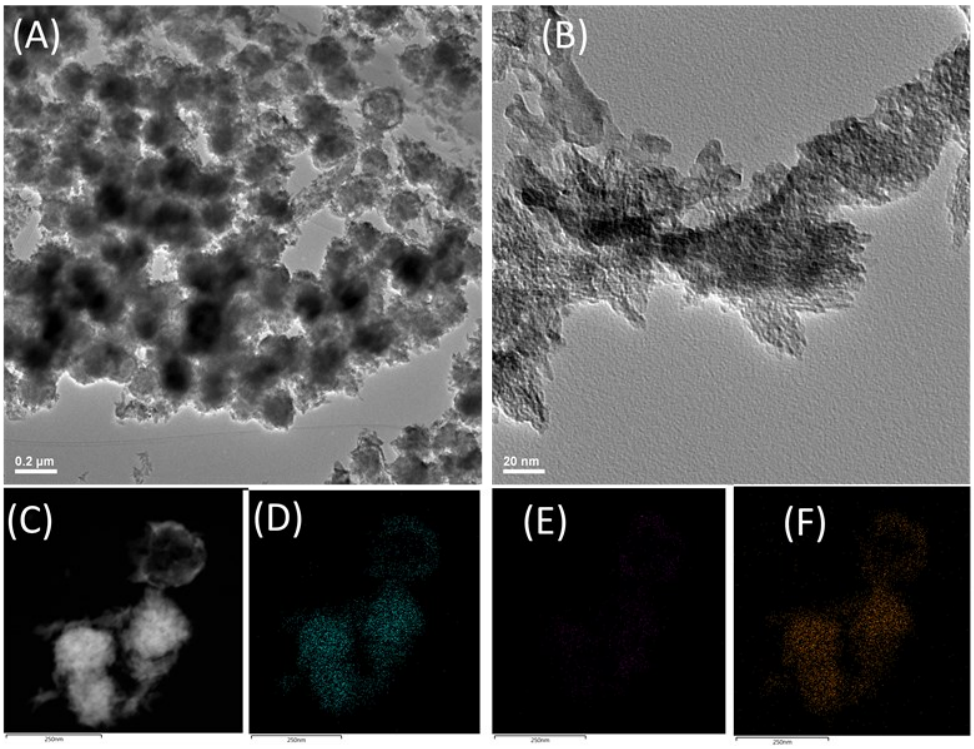

Fig. S12. (A) Low- and (B) high-magnification TEM, and (C) HAADF-STEM images of MnO@TiO_2/RGO-acid-72h nanocomposites. (D) Ti, (E) Mn and (F) O maps of the MnO@TiO_2/RGO-acid-72h nanocomposites in (C).

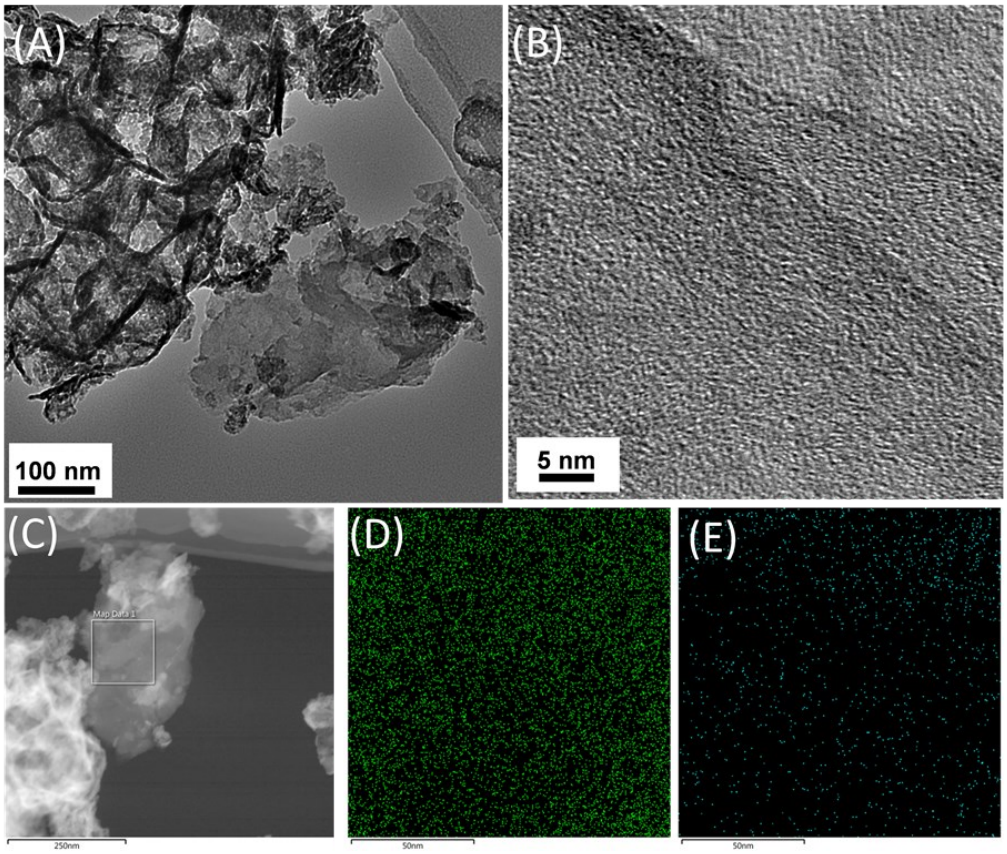

Fig. S13. (A) TEM, (B) HRTEM and (C) HAADF-STEM images of MnO@TiO_2/RGO-acid-S nanocomposites. (D) C and (E) S maps of the boxed MnO@TiO_2/RGO-acid-S nanocomposites in (C).

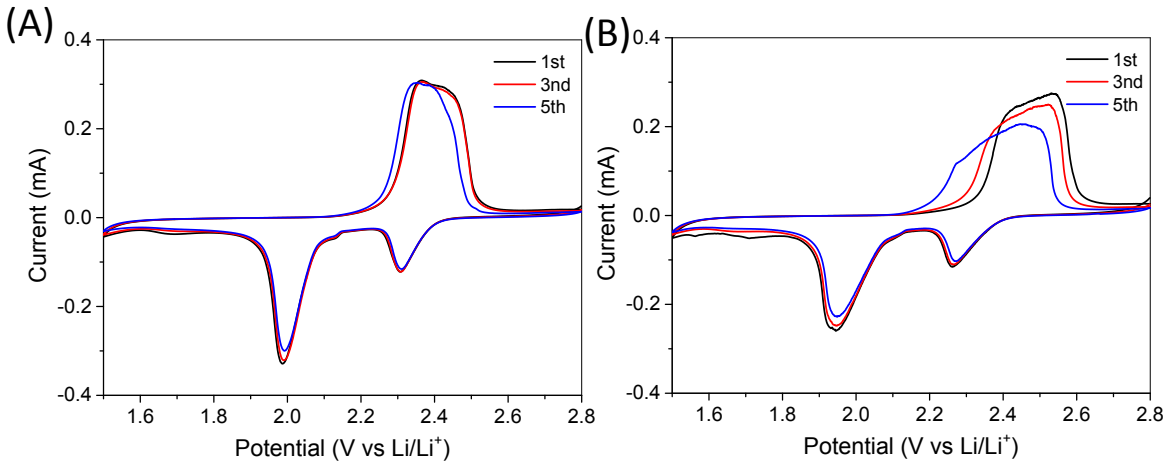

Fig. S14. CV profiles of (A) MnO@TiO_2/RGO-S and (B) MnO@TiO_2-S. A scan rate of 0.05 mV/S was used over a potential range of 1.5–2.8 V (versus Li/Li^+).

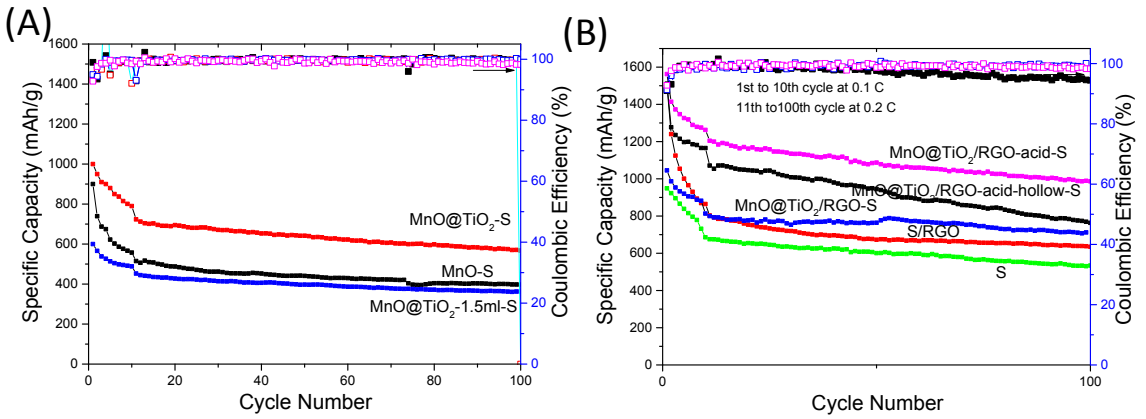

Fig. S15. (A) Cycling performance of MnO-S, and MnO@TiO_2-S and MnO@TiO_2-1.5ml-S nanocomposites at room temperature. (B) Cycling performance of MnO@TiO_2/RGO-S, MnO@TiO_2/RGO-acid-S and MnO@TiO_2/RGO-acid-hollow-S nanocomposites, S/RGO, and S nanocrystals at room temperature. Closed square: specific capacity; open square: Coulombic efficiency.

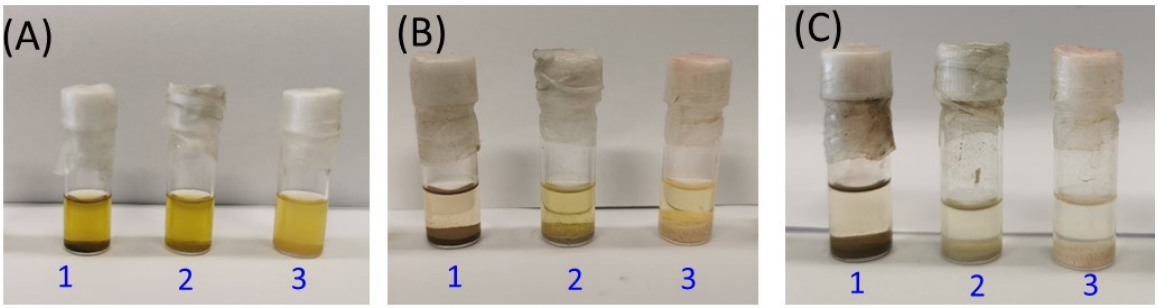

Fig. S16. Photographs of Li_2S_6 solution with DOL/DME solvent (A) before, and (B) 3 h and (C) 12 h after introducing (1) MnO nanoparticles, (2) amorphous TiO_2, and (3) commercial crystalline TiO_2.

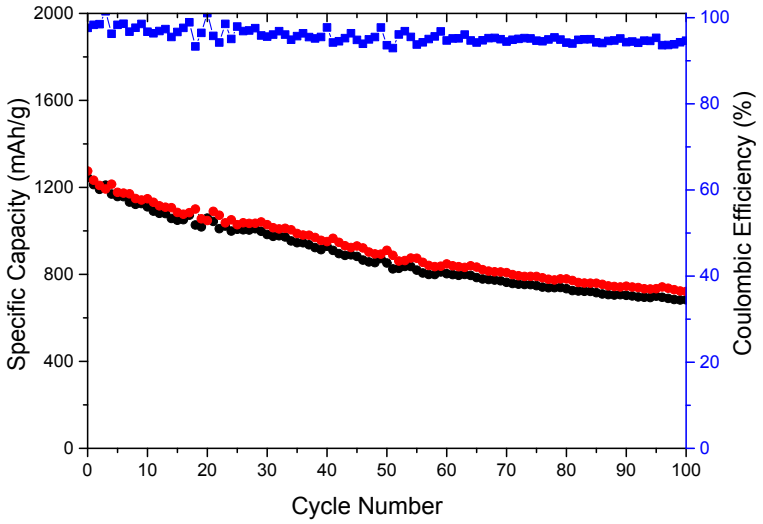

Fig. S17. Cycling performance of MnO@TiO_2-acid-S nanocomposites with 3 mg/cm^2 sulfur loading at room temperature: specific capacity at 0.2 C during (●) charging and (●) discharging, and Coulombic efficiency (■).

References

1. W. Li, Z. Gong, X. Yan, D. Wang, J. Liu, X. Guo, Z. Zhang, G. Li, *J. Mater. Chem. A* **2020**, *8*, 433–442.
2. Z. Ye, Y. Jiang, J. Qian, W. Li, T. Feng, L. Li, F. Wu, R. Chen, *Nano Energy* **2019**, *64*, 103965.
3. L. Hu, C. Dai, H. Liu, Y. Li, B. Shen, Y. Chen, S. Bao, M. Xu, *Adv. Energy Mater.* **2018**, *8*, 1800709.
4. C. Ye, L. Zhang, C. Guo, D. Li, A. Vasileff, H. Wang, S. Qiao, *Adv. Funct. Mater.* **2017**, *27*, 1702524.